J Solid State Electrochem (2012) 16:1561–1569
DOI 10.1007/s10008-011-1561-y

ORIGINAL PAPER

A comparative study of sequentially layer-deposited and co-deposited Co–Mn oxides as potential redox capacitors

Fereydoon Gobal · Sanaz Jafarzadeh

Received: 2 August 2011 / Revised: 13 September 2011 / Accepted: 20 September 2011 / Published online: 7 October 2011

Abstract Layers of cobalt and manganese oxides were co-deposited or deposited on top of each other or next to each other by potentiostatic method onto stainless steel substrate. Deposition potentials of 1 and −1 V for the anodic and cathodic depositions were employed. Specific capacitance values in the range of 38.5–78 F g^{-1} were found with cobalt oxide on top of manganese oxide having the lowest and manganese oxide on top of cobalt oxide having the highest capacitances. The usefulness of the electrodes was characterized by cyclic voltammetry, charge–discharge cycling, and electrochemical impedance spectroscopy in 2 M NaOH electrolyte for redox supercapacitor applications. The latter presented the best charge/discharge behavior with no voltage drop due to lower ohmic resistance in prepared substrate; although the steadiest current observed in the course of voltammetry was due to the former. The evaluated double layer and specific capacitances for co-deposited sample according to the impedance studies were 1.75 and 47.5 F g^{-1}, respectively, being in good agreement with voltammetric measurements.

Keywords Co–Mn oxides · Layered oxides · Potentiostatic deposition · Specific capacitance · Supercapacitor

Introduction

Supercapacitors have an ever-expanding array of applications as portable electronics continue to expand in popularity. Supercapacitors or electrochemical capacitors take advantage of (1) the charge stored in the electrochemical double layer and (2) the charge stored due to Faradic processes [1–4] that can provide high-specific capacitance around 1,000 F g^{-1}.

The electrodes of electrochemical redox supercapacitors consist of electroactive materials with several oxidation states. These types of capacitors are currently under extensive investigation because of both high power and high energy characteristics [1–4]. Hydrous RuO_2 providing capacity of around 720 F g^{-1} in aqueous acidic electrolyte is the best system so far realized [5, 6] where charge/discharge is accompanied by the release/uptake of proton to/from the electrolyte [7]. Although RuO_2 gives high-specific capacitance, it has disadvantages of high cost and toxicity. In search of inexpensive alternatives for RuO_2, manganese oxide prepared by both chemical and electrochemical methods was found to possess acceptable capacities [8, 9]. Hu et al. have shown that amorphous ($\alpha - MnO_2 \cdot nH_2O$) having high-specific capacitance (SC) of 265 F g^{-1} can be synthesized by anodic deposition [9]. Cathodic electrophoretic deposition method has been developed for the deposition of manganese oxide films in presence of phosphate ester (PE) as dispersant show (SC) of 377 F g^{-1} [10]. Cobalt oxide thin film has been prepared by various methods such as spray pyrolysis (SC of 74 F g^{-1}), sputtering, chemical vapor deposition, pulse laser deposition, sol–gel process, electrodeposition, successive ionic layer adsorption and reaction (SC of 165 F g^{-1}) and hydrothermal process (SC of 237 F g^{-1}) on a variety of substrates. Each deposition method has its own advantages [11–14].

The purposes of the present study is to potentiostatically deposit mixed cobalt–manganese oxides and study their electrochemical capacitance where methods of X-ray diffraction (XRD and energy dispersive X-ray analysis (EDX)) have been used for materials characterization, and

F. Gobal · S. Jafarzadeh (✉)
Department of Chemistry, Sharif University of Technology,
P.O. Box 11365-9516, Tehran, Iran
e-mail: jafarzadeh@mehr.sharif.ir

cyclic voltammetry (CV) and chronoamperometry have been employed for electrochemical studies.

Experimental

Cobalt and manganese nitrates and NaOH used in this work were analytical grade Merck products and water was deionized. The Co–Mn oxides were deposited onto a commercially available stainless steel (SS; grade 304) foil of 0.2 mm thickness by chronoamperometric method where deposition potentials of 1 and −1 V for the anodic and cathodic depositions were employed, respectively. SS foil having geometric area of 1 cm^2 was polished with emery paper (grit number 220) to a rough finish, washed free of emery particles and air dried prior to electrodepositions. The electrochemical cell used in this study is a conventional three-electrode cell with the deposited mixed oxides forming the working, a Pt ribbon was the auxiliary electrode and a saturated calomel electrode (SCE) was used as the reference electrode. All potentials are reported against SCE.

The electrodeposited films were washed in running distilled water and dried at room temperature. All electrochemical depositions and capacitance measurements were performed by Behpajoo 2,063+ galvanostat/potentiostat. 2 M NaOH solution was used in electrochemical studies.

XRD patterns (Co Kα line) were obtained using a Philips (θ–2θ configuration) diffractometer (model expert MPD) for the 2θ range of 10°–80°. Chemical compositions were determined by EDX in a scanning electron microscope (VEGA\\Tescan).

Four types of Co–Mn oxides were deposited. (1) (CM) which is a mixed oxide was deposited onto SS by cathodic deposition at −1 V/SCE for 900 s from a solution of 2 M $MnSO_4 \cdot 5H_2O$ + 2M $Co(NO_3)_2 \cdot 6H_2O$ at pH ~6. (2) The second sample (M|C) was cathodically deposited at −1 V/SCE from a 2M $Co(NO_3)_2 \cdot 6H_2O$ solution onto the surface of manganese oxide previously anodically deposited on SS at 1 V/SCE from a 2 M solution of $MnSO_4 \cdot 5H_2O$. (3) The third sample (C|M) is manganese oxide anodically (+1 V/SCE) electrodeposited onto the previously deposited (at −1 V/SCE) cobalt oxide surface. (4) The fourth sample (C–M) was cathodically (−1 V/SCE) electrodeposited cobalt oxide next to the anodically (+1 V/SCE) electrodeposited manganese oxide on (SS). To prepare the neighboring deposits, one half of the length of a SS ribbon is first covered by Mn oxide followed by dipping the clean half into the Co bath and depositing Co oxide ensuring a marginal contact (overlap) at the boundaries. The surfaces of electrodes were 1 cm^2 and the weights of all deposited materials were ~2 mg which were weighed by an analytical balance. The samples are schematically presented in Fig. 1.

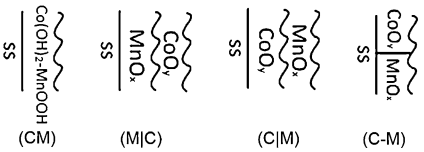

Fig. 1 Mixed oxides prepared samples

Results and discussion

Figure 2 presents the XRD pattern of (CM), (M|C), and (C|M). There are some sharp peaks at 52°, 77°, and 90° that are due to stainless steel substrate and are observed in all patterns due to the low thicknesses of the mixed oxides films. Figure 2a shows the XRD pattern of (CM) which corresponds to a mixture of Co $(OH)_2$ and MnOOH. The pattern comprises of one sharp peak appearing at 23.5° and three broad peaks at θ values of around 45.8°, 59.6°, and 77.5°. The pattern of Co $(OH)_2$ in Fig. 2a consists of four peaks appearing at mentioned angles. The first two peaks (23.5° and 45.8°) are related to d spacings that are multiples of each other due to multiple reflections from the basal planes and are indexed as (001) and (002) planes. The third and fourth peaks have similar "saw-tooth" shapes, with a sharp rise at the low-angle side and pronounced asymmetry on the high-angle side. This suggests that they belong to a group of planes different from (00*l*) planes [15, 16]. These peaks are indexed as (102) and (110) [17]. The XRD pattern corresponds to the well-known form of hexagonal crystalline Co $(OH)_2$ [18]. Previously reported XRD patterns of Co $(OH)_2$ prepared by precipitation methods, show stronger (00*l*) reflections compared to other reflections which is not the case in Fig. 2a. This is due to the nanosize of α-Co $(OH)_2$ layers along the basal planes, which results in loss of intensity of the (00*l*) reflections [18]. The XRD pattern for MnOOH is seen in Fig. 2a. The

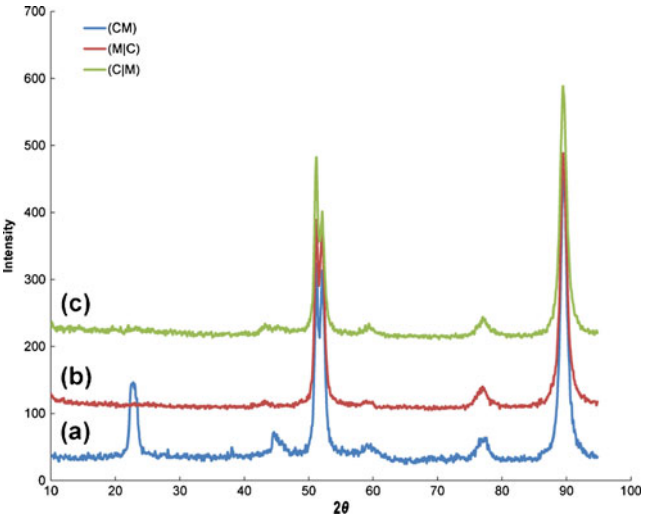

Fig. 2 XRD pattern of the **a** (CM), **b** (M|C), and **c** (C|M)

peak at 22.2° is dominant. According to the powder diffraction file (PDF#18-0804), this peak can be attributed to the tetragonal crystalline phase of β-MnOOH (feitknechite) (002) [19–21].

Figures 2b and c show XRD patterns of (M|C) and (C|M). It is confirmed that there is a deposited layer with structure of Mn oxide (MnO_2) in (M|C) and Co_3O_4 in (C|M). To discover the crystallinity of the as-prepared MnO_2 product, XRD analysis was undertaken, and the pattern is shown in Fig. 2b. The two characteristic peaks (311) and (400), at 43.3° and 52.8° clearly presented, were confirmed to be due to cubic crystalline of MnO_2 (PDF# 42-1169). The weak broad peaks observed in the XRD pattern suggest the sample is in a poorly crystalline state with only a short-range crystallinity [22]. Two broadened diffraction peaks are according to (PDF# 42-1169) strong indication of nanocrystals in MnO_2 [23, 24]. The XRD pattern of (C|M; Fig. 2c) showed the formation of cobalt oxide with cubic structure. A peak appearing at 52.8° is attributed to a major reflection due to (400) plane. Another peak at 44.9° corresponding to (222) plane and at 77.4° regarding to (440) plane are observed with lower scattering intensities. No other additional peak corresponding to other phases of cobalt oxide is seen to have been emerged [7]. There are no peaks corresponding to Co presence in (M|C) and Mn presence in (C|M) which had been deposited on samples at the second stages of preparation. The existence of Mn in (C|M) has been confirmed by energy dispersive spectroscopy (EDS) and is probably in amorphous state. The amorphous natures of the layers will be discussed later.

Elemental analysis was performed by EDS and the results for (CM) sample are presented in Fig. 3. Strong peaks due to Mn and Co were observed in the spectrum with the atomic ratio of 33.98:39.56 (Mn/Co), which confirms the presence of Mn and Co that have crystalized in MnOOH and $Co(OH)_2$ structures, respectively, according to the obtained XRD data (Fig. 2a). It should be mentioned that XRD and scanning electron microscopy (SEM) studies have been carried out using the samples already undergone electrochemical tests.

The mechanism for (CM) sample formation is probably as follows:

$$M^{2+}+H_2O+2e^- \rightarrow M(OH)_2+H_2; M = \text{Co or Mn(formation)} \quad (1)$$

$$M(OH)_2+OH^- \rightarrow MOOH+H_2O+e^-(\text{activation}) \quad (2)$$

and the reaction beyond the redox peaks at higher potential can be expressed as [17]:

$$COOH + OH^- \rightarrow CoO_2+H_2O+e^- \quad (3)$$

Reaction (2) occurs during the first CV cycle in alkaline bath (2 M NaOH) and is accompanied by the color change of (CM) after the first CV cycle.

EDS result for (C|M) sample is presented in Fig. 4. Strong peaks due to Mn and Co are observed in the spectrum corresponding to the atomic ratio of 70.91:7.33 (Mn/Co), where the apparent cobalt content is contributed from the electrodeposited underlayer.

(C|M) is considered to be mainly formed by the electrochemical and chemical reactions shown below:

$$Co^{2+}+H_2O \rightarrow Co(OH)_2+H_2(\text{inthe under cathodically deposited layer}) \quad (4)$$

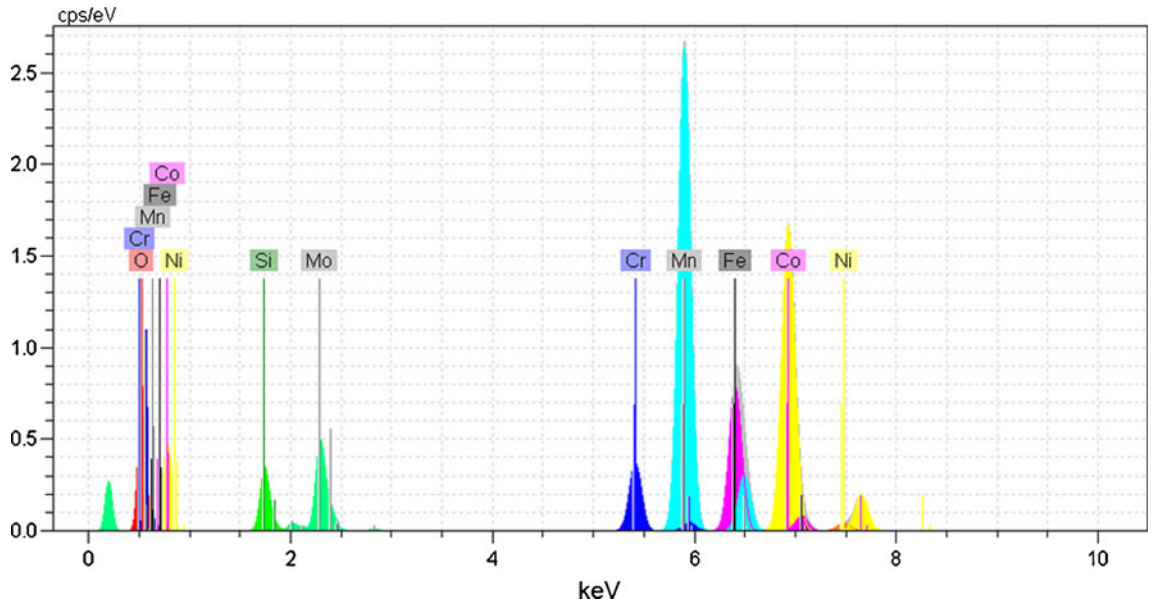

Fig. 3 The EDS of (CM)

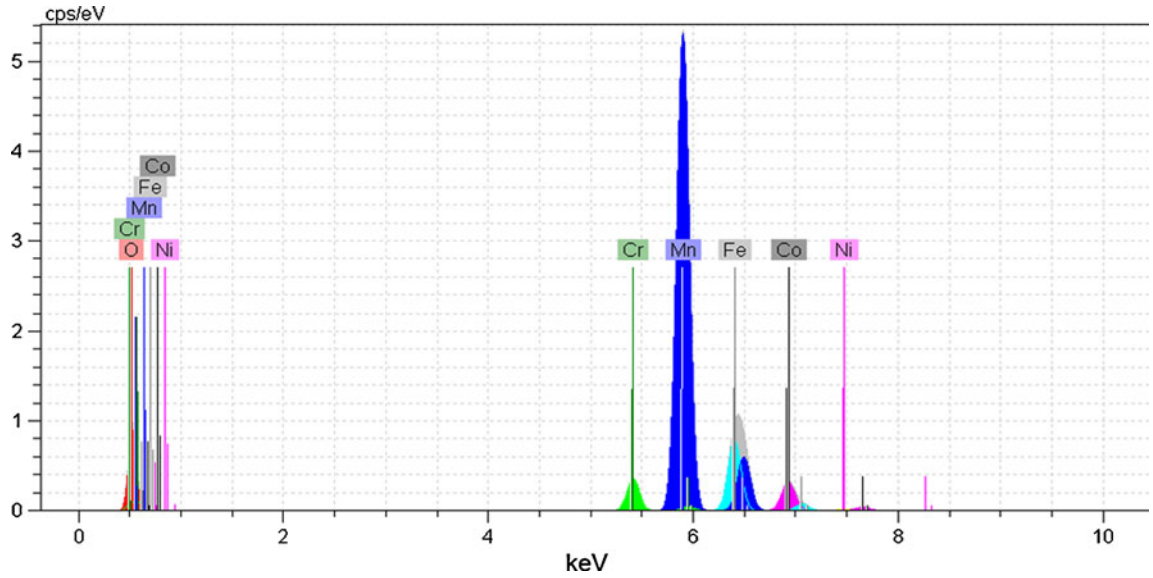

Fig. 4 The EDS of (C|M)

$$Mn^{2+}+2H_2O \rightarrow MnO_2+4H^{+}+4e^{-}\text{(in the top anodically deposited layer)} \quad (5)$$

Co $(OH)_2$ in the presence of oxygen is converted to Co_3O_4:

$$6Co(OH)_2+O_2 \rightarrow 2Co_3O_4+6H_2O \quad (6)$$

The surface morphology of the electrodeposited (C|M) thin film was investigated by scanning electron microscopy. Figure 5 shows the SEM image of (C|M) sample. The deposited film is amorphous and consists of islands separated by cracks of around 500 nm wide. The surface is fairly uniform in every island. As it is seen, the deposited underlayer is observed by SEM and Mn oxide particles have deposited on the previous layer. Both deposited layers thus come in contact with the electrolyte in the course of the electrochemical studies.

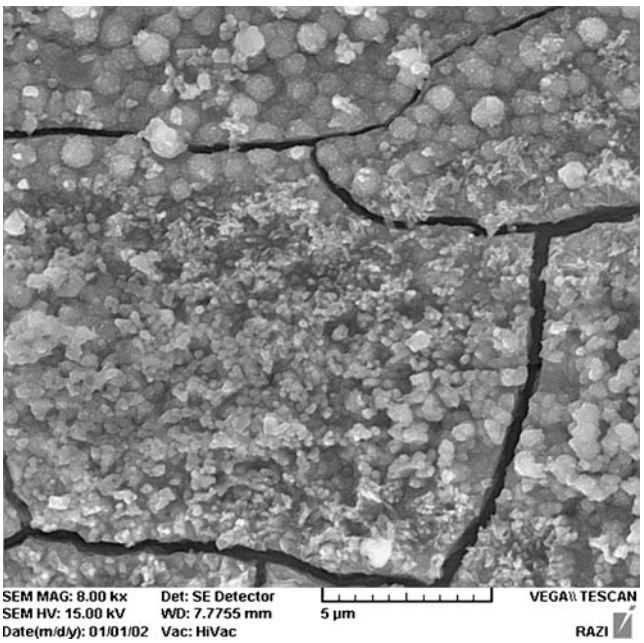

Fig. 5 The SEM images of (C|M) electrode at magnification of ×8,000

Figure 6 shows typical CVs of (CM) electrodes in 2 M NaOH electrolyte at different scan rates. The potential window of (CM) is around 0.7 V that it is considerably wider compared to Co $(OH)_2$ [18] and cobalt oxide samples prepared by other methods [14, 25–27] but it is narrower than the potential window of MnOOH. Therefore, it is found that cobalt hydroxide presence in (CM) is a limiting agent in the width of the potential window.

The voltammograms are almost symmetrically located along the potential axis and are typical of capacitive behavior. It is generally known that the charge stored in a double layer is rather low and high currents as seen in the CVs (Fig. 6) could not be attributed to double-layer charge/discharge processes.

The average capacitance (C) is calculated using:

$$C = \frac{I}{\frac{dV}{dt}} \quad (7)$$

where, I is the mean current along the voltammogram and $\frac{dV}{dt}$ is the potential sweep rate. The specific capacitance (F g^{-1}) of (CM) electrode is obtained through dividing C by its respective weight.

The specific capacitance is decreased from 80 to 50 F g^{-1} as the potential scan rate is increased from 5 to

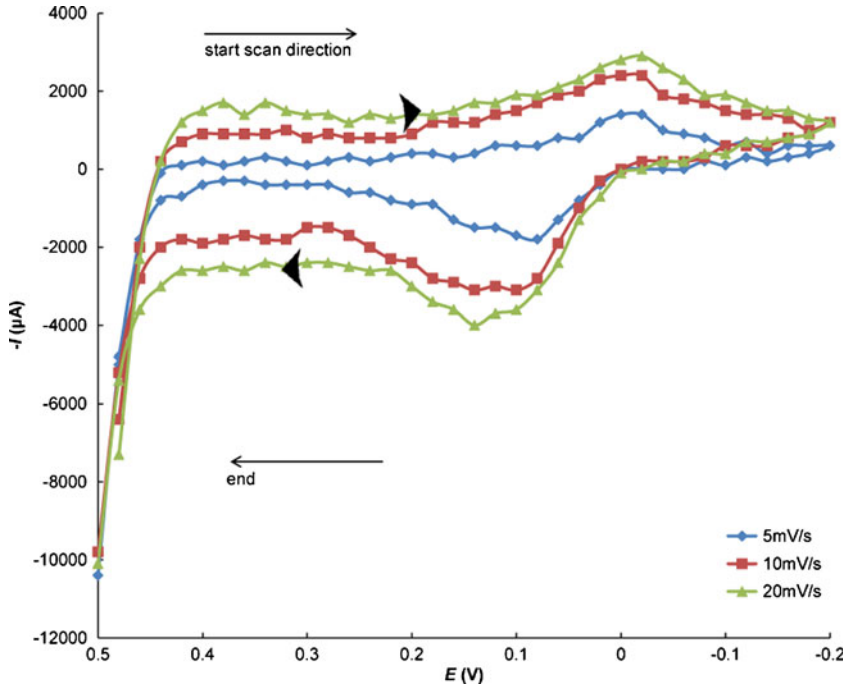

Fig. 6 Cyclic voltammogram of (CM) in 2 M NaOH electrolyte with 5, 10, 20 mV s^{-1} scan rates

20 mV s^{-1}. The decrease in capacitance with the scan rate is attributed to the presence of inner active sites which cannot be accessed at higher scan rates, probably due to the diffusion limited transfer of OH^- to such sites [28] and some sites fail to undergo redox processes at high potential sweep rates. Hence, the specific capacitance obtained at the slowest scan rate is believed to be close to that of full utilization of the electro-active material [18].

Figure 7 presents the charge–discharge cyclic voltammograms of (CM), (M|C), (C|M), and (C–M) electrodes in 2 M NaOH electrolyte at 20 mV s^{-1} scan rate. It is observed that the behavior of CVs do not exactly correspond to the expected CVs for supercapacitors since the capacitive behavior in these samples is due to faradic capacitance (not double-layer capacitance) and it is common in Faradic capacitances.

As it is seen in Fig. 7, the underlayer deposits, Mn oxide in (M|C) or Co oxide in (C|M), have profound effect on the measured capacitance. Comparing CVs of (CM) and (M|C), Fig. 7, shows improvements in the potential window from 0.7 to 1 V, much more steady current throughout and symmetry of the voltammogram in (M|C) due to MnO_2 presence in comparison with MnOOH presence in (CM). On the other hand, although higher currents have been realized in (C|M) sample, the width of the potential window has been scarified.

Therefore, it is concluded that Mn oxide underlayer improves the operating potential window while Co oxide underlayer improves the current density and increases the charge stored. (C–M) which exposes both cobalt oxide and MnO_2 surfaces to the electrolyte, shows a behavior similar to prepared cobalt oxide in Fig. 8 and it is because of cobalt oxide presence in (C–M) that create a substrate with lower resistance and higher current density and it is chosen as the selective path for charging process. C_S (capacitance per mass of active material) values for (CM), (M|C), (C|M), and (C–M) were found to be 48, 38.5, 78, and 40.6 F g^{-1}, respectively, where measurements have been made at 20 mV s^{-1} potential sweep rate. These values of C_S are comparable with the values reported in the literature [18, 20–23] for various other low-cost metal oxides.

The charge–discharge behaviors of (M|C) electrodes under galvanometric mode at constant currents of ±1 mA are presented in Fig. 9. The discharge profiles usually consist of two parts: a sharp potential drop (often very small) due to internal resistive component of materials is followed by the discharge of a capacitive component. (CM) and (C|M) samples do not show any significant internal resistance drop and their charge–discharge behavior were close to ideal that must be because of much lower internal resistance of Co_3O_4 (1.5×10^3 Ω cm) [29] in (C|M) and Co $(OH)_2$ (1.29 Ω) [30] in (CM) samples in comparison with internal resistance of MnO_2 (5.5×10^5 Ω cm) [31] in (M|C). This high-specific resistance is due to the fact that the crystalized Mn oxide layers are lying parallel to the electrode surface, which was disclosed by cross-sectional transmission micrography and in-plane X-ray diffraction measurements [32]. This leads to a difficulty in electron conduction along a direction perpendicular to the substrate surface and does not allow easy access of charge-

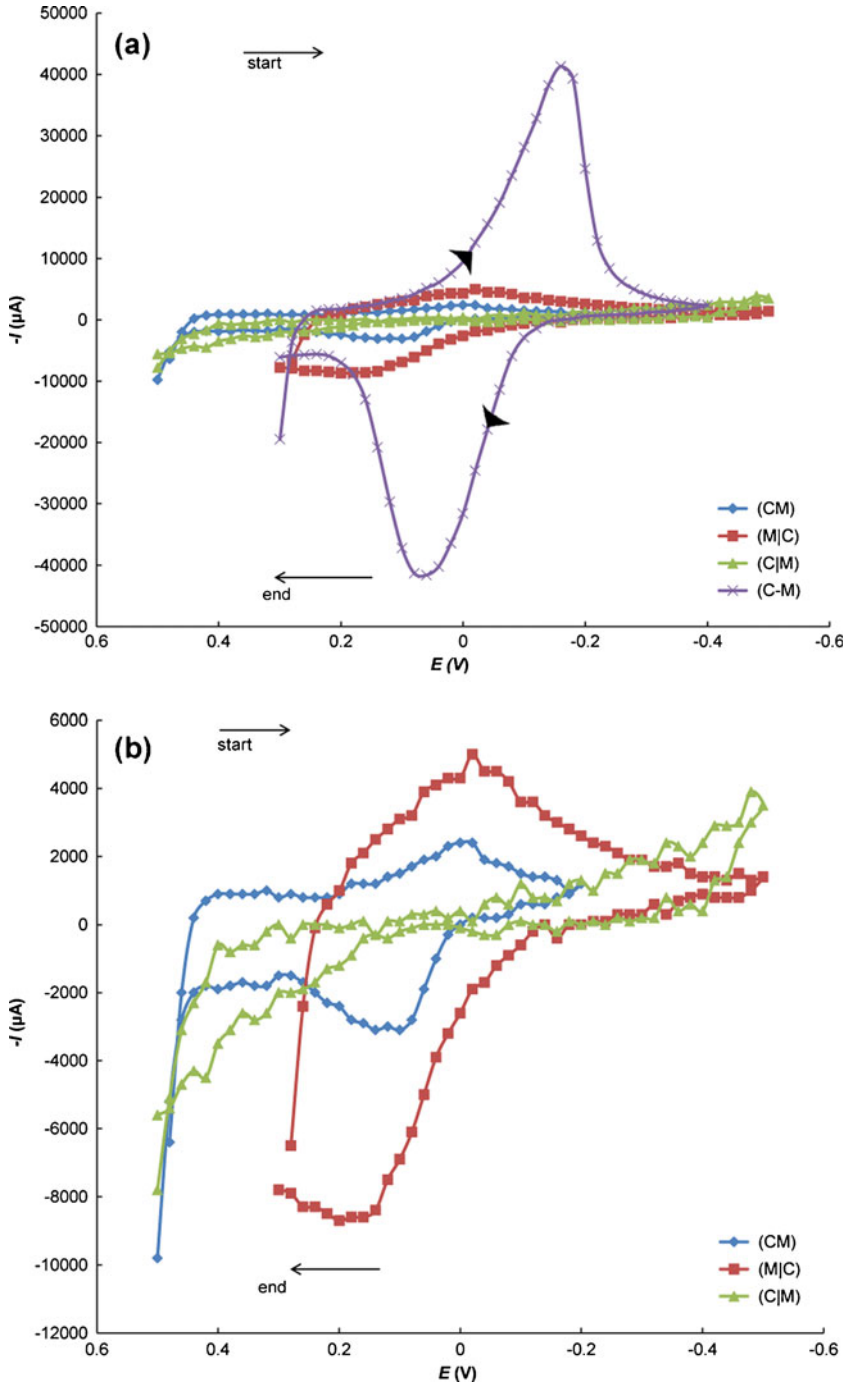

Fig. 7 Cyclic voltammogram of **a** (CM), (M|C), (C|M), and (C–M) and **b** zoomed in of (CM), (M|C), and (C|M) in 2 M NaOH electrolyte at 20 mV s^{-1} scan rate

compensating cations in solution to the inter layer surface. Voltage drop in Fig. 9 for (M|C) sample is around 600 mV which is close to calculated voltage drop according to the internal resistances. Thickness of sample is 10^{-3} cm, surface area of electrode is 1 cm^2 in (M|C), and therefore, ohmic drop at 1 mA current is calculated to be 550 mV.

However, it should be mentioned that (C–M) behaves similar to cobalt oxide and it is because of lower specific resistance of cobalt oxide compared to MnO_2. It causes the charge–discharge process to choose the path with higher conductivity and it has the main role in (C|M) and (C–M) charge–discharge processes.

The specific capacitances of the electrodes are evaluated [33, 34] using:

$$C = \frac{Q}{\Delta V \times m} = \frac{I \times \Delta t}{\Delta V \times m} \tag{8}$$

Where C (F) is capacitance, I (A) is current in the course of charge/discharge processes, Δt (sec) is the charge/discharge time, ΔV (V) being the potential window and m (g) is the

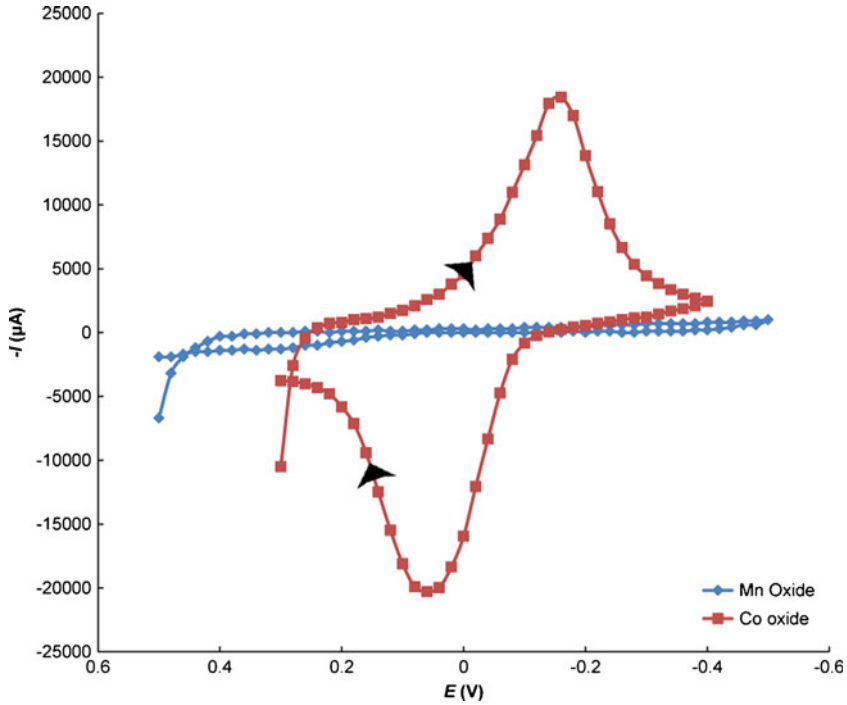

Fig. 8 Cyclic voltammogram of Co Oxide and Mn oxide in 2 M NaOH electrolyte with 20 mV s^{-1} scan rate

mass of the electrodeposited materials. From charge–discharge profiles the specific capacitances are estimated to be 50, 37, 80, and 41.6 F g^{-1} for (CM), (M|C), (C|M), and (C–M), respectively, which are comparable with the values derived from the CV studies.

The SCs are ordered as:

$$SC(C|M) > SC(CM) > SC(C-M) > SC(M|C)$$

It was found that the best result is obtained when the mixed-metal oxide components are deposited on top of each other and the underlayer is metal oxide with higher specific conductance (Co_3O_4). It was confirmed by XRD studies that the co-deposited metal oxides ((CM)) structure is different from the samples formed by subsequent depositions ((C|M) and (M|C)). It is conceivable that in consecutive depositions the primary deposited layer leads

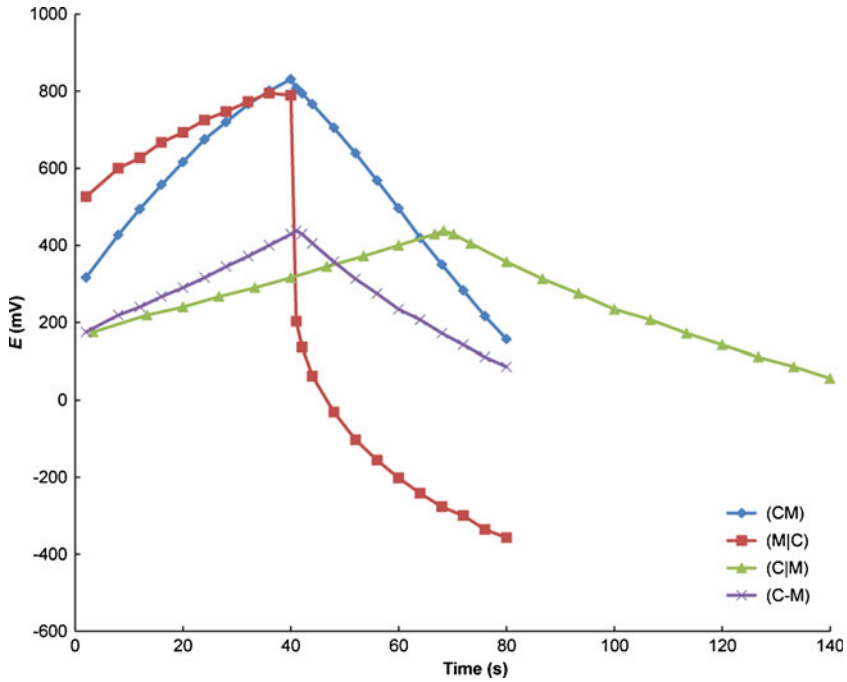

Fig. 9 The charge and discharge curves of Co–Mn oxides in 2 M NaOH electrolyte. The charging current was 1 mA cm^{-2}

the secondary layers to be formed with an amorphous structure, so, an amorphous structure of MnO_2 (α-MnO_2) forms the top layer of (C|M) that has been known to show good capacitance. Also, the deposited underlayer is not completely covered (according to the SEM image of (C|M)) and there are interfaces between the electrolyte and both the deposited upperlayers and underlayers. Both wide potential window of MnO_2 and high-specific conductance of Co_3O_4 are simultaneously observed in (C|M) sample.

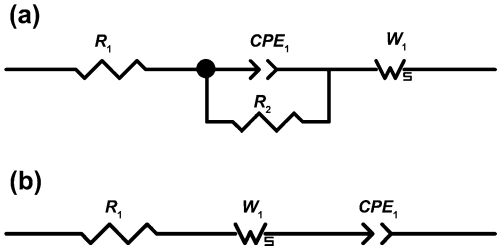

Fig. 11 Equivalent circuit for (CM) at **a** −0.2 and 0 V, **b** 0.2 V

Impedance studies

Figure 10 presents Nyquist plots for (CM)/NaOH at −0.25, 0, and 0.2 V/SCE in the range of frequencies from 100 kHz to 20 mHz, where Z′ and Z″ are the real and imaginary parts of the impedance, respectively. While the ideal capacitor exhibits a vertical line in the Nyquist plot, the electrochemical capacitor starts with a 45° impedance line and approaches an almost vertical line only at low frequencies [35].

The nonvertical slope of the low frequency impedance can be accounted for by replacing the capacitance with a constant phase element (CPE) where $j\omega$ term is replaced by $(j\omega)^p$, with $0<p<1$, and where $p=1$ represents an ideal capacitor.

The equivalent circuit for (CM) at −0.25 and 0 V/SCE are shown in Fig. 11a which has best fits the experimental findings.

The evaluated specific capacitances according to the equivalent circuit and fitted data by ZView software are 1.75 and 47.5 F g^{-1} at −0.25 and 0 V/SCE, respectively. It was found that at −0.25 V/SCE, the capacitor has not yet been charged up and CPE value is due to double-layer capacitance. By shifting to charging potentials (0 V/SCE), the evaluated capacitance is close to the values obtained in charge/discharge experiments.

The equivalent circuit compatible with Nyquist plot at 0.2 V/SCE is presented in Fig. 11b. Apparently, shifting the potential to more positive values tends to increase the parallel resistance and causes R_2 to disappear from the equivalent circuit in Fig. 11a. It should be mentioned that the power of CPE, CPE-p, has been found to be 0.93 and 0.90 ($0<p<1$) at 0 and 0.2 V, respectively, that shows (CM) behaves close to an ideal capacitor.

The specific capacitance can be obtained by another numerical method according to the following:

$$Z'' = \frac{1}{(C\omega)^p} \tag{9}$$

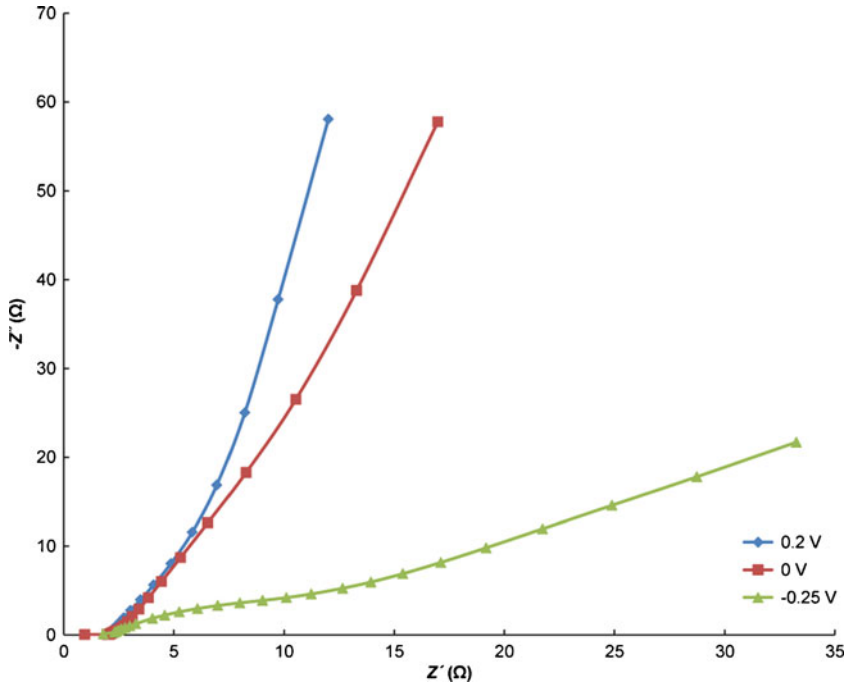

Fig. 10 Nyquist plots for the (CM) electrode in 2 M NaOH solution at −0.25, 0, and 0.2 V

At frequency equal to 20 mHz, Z' equal to 58.06 Ω and power of CPE, p, equal to 0.9 and the specific capacitance was calculated to be 48 F g^{-1} which is in accord with other measurements.

Conclusion

Manganese–cobalt oxides composite electrodes with different anodic and cathodic electrodepositions sequences have been prepared. A specific capacitance of 78 F g^{-1} has been obtained at the current density of 1 mA in 2 M NaOH aqueous solution for (C|M) sample where Co_3O_4 is the underlayer and has caused an amorphous structure of MnO_2 to be deposited as the upperlayer. (C|M) electrode has good charge/discharge properties without any significant ohmic drop in the discharge process due to low electrical resistance of Co_3O_4 in (C|M). Also, it was concluded that (C–M) which exposes both cobalt oxide and MnO_2 surfaces to the electrolyte, shows a behavior similar to the cobalt oxide and it is because of cobalt oxide presence in (C–M) that tends to lower the resistance promote higher current density and provides as the path for charging process. The evaluated double layer and specific capacitances for (CM) according to the impedance studies were 1.75 and 47.5 F g^{-1}, respectively, which conforms strongly with obtained C_S from cyclic voltammogram and chronopotentiometric studies.

Acknowledgment The authors wish to express thanks to the office of vice chancellor of research of Sharif University of Technology for the financial support.

References

1. Conway BE (1999) Electrochemical supercapacitors—scientific fundamentals and technological applications. Kluwer/Plenum, New York
2. Conway BE (1991) Electrochem Soc 138:1539–1548
3. Burke AF, Murphy TC (1995) Mater Res Soc 393:375–382
4. Sarangapani S, Tilak BV, Chen CP (1996) Electrochem Soc 143:3791–3799
5. Zheng JP, Jow TR (1995) Electrochem Soc 142:L6–L8
6. Kim HH, Kim KB (2001) Electrochem Solid State Lett 4: A62–A64
7. Kotz R, Carlen M (2000) Electrochem Acta 45:2483–2498
8. Pang SC, Anderson MA, Chapman TW (2000) Electrochem Soc 147:444–450
9. Hu CC, Tsou TW (2002) Electrochem Commun 4:105–109
10. Li J, Zhitomirsky I (2009) Colloid and Surf A: Physicochem Eng Asp 348:248–253
11. Calva E, Flores J, Huerta L, Avila A, Lo'pez M (2006) Sol Eng Mater Sol Cell 90:2523–2531
12. Casella IG, Gatta M (2002) Electroanal Chem 534:31–38
13. Kandalkar SG, Gunjakar JL, Lokhande CD (2008) Appl Surf Sci 254:5540–5544
14. Zhang GQ, Zhao YQ, Tao F, InLi H (2006) Power Source 161:723–729
15. Zhang ML, Liu ZX (2002) Chin J Inorg Chem 5:513–517
16. Hosono H, Fujihara S, Honma I, Ichihara M, Zhou H (2006) Power Source 158:779–783
17. Gupta V, Kuhasara T, Toyama H, Gupta S, Miura N (2007) Electrochem Commun 9:2315–2319
18. Djurfors B, Broughton JN, Brett MJ, Ivey DG (2005) Acta Mater 53:957–965
19. Feng XH, Tan WF, Liu F, Huang QY, Liu XW (2005) Sci China. Ser D: Earth Sci 48:1438–1451
20. Luo JA, Zhang QH, Suib SL (2000) Inorg Chem 39:741–747
21. Zhou F, Zhao XM, Yuan CG, Xu H (2007) Mater Sci 42:9978–9982
22. Chang JK, Tsai WT (2003) Electrochem Soc 150:A1333–A1338
23. Jeong YU, Manthiram A (2002) Electrochem Soc 149:A1419–A1422
24. Sivakkumar SR, Ko JM, Kim DY, Kim BC, Wallace GG (2007) Electrochem Acta 52:7377–7385
25. Liu KC, Anderson MA (1996) Electrochem Soc 143:124–130
26. Srinivasan V, Weidner JW (1997) Electrochem Soc 144:L210–L213
27. Lin C, Ritter JA, Popov BN (1998) Electrochem Soc 145:4097–4103
28. Chang KH, Hu CC (2004) Electrochem Soc 151:A958–A964
29. Shinde VR, Mahadik SB, Gujar TP, Lokhande CD (2006) Appl Surf Sci 252:7487–7492
30. Yuan C, Zhang X, Gao B, Li J (2010) Electrochem Acta 56:115–121
31. Czech Noise Research Laboratory (2000) Tantalum capacitors as a metal–insulator–semiconductor structure. http://www.kyocera.co.jp/prdct/electro/pdf/technical/cap_mis00.pdf
32. Nakayama M, Kanaya T, Inoue R (2007) Electrochem Commun 9:1154–1158
33. Fusalba F, Gouerec R, Villers D, Belanger D (2001) Electrochem Soc 148:A1–A6
34. Park JH, Park OO (2002) Power Source 111:185–190
35. Sun W, Hsu A, Chen R (2011) Power Source 196:627–634